Interfacial Nanobubbles Are Leaky: Permeability of the Gas/Water Interface

Sean R. German,[†] Xi Wu,[‡,§] Hongjie An,[∥] Vincent S. J. Craig,[∥] Tony L. Mega,[†] and Xuehua Zhang[‡,§,*]

[†]Revalesio Corporation, 1200 East D Street, Tacoma, Washington 98421, United States, [‡]Department of Chemical and Biomolecular Engineering and [§]School of Chemistry, University of Melbourne, Parkville, Victoria 3010, Australia, and [∥]Department of Applied Mathematics, Research School of Physical Sciences and Engineering, Australian National University, Canberra ACT 0200, Australia

ABSTRACT Currently there is no widespread agreement on an explanation for the stability of surface nanobubbles. One means by which several explanations can be differentiated is through the predictions they make about the degree of permeability of the gas—solution interface. Here we test the hypothesis that the gas—solution interface of surface nanobubbles is permeable by experimental measurements of the exchange of carbon dioxide. We present measurements by attenuated total reflection Fourier transform infrared (ATR-FTIR) and atomic force microscopy (AFM), demonstrating that the gas inside surface nanobubbles is not sealed inside the bubbles, but rather exchanges with the dissolved gas in the liquid phase. Such gas transfer is measurable by using the infrared active gas CO_2. We find that bubbles formed in air-saturated water that is then perfused with CO_2-saturated water give rise to distinctive gaseous CO_2 signals in ATR-FTIR measurements. Also the CO_2 gas inside nanobubbles quickly dissolves into the surrounding air-saturated water. AFM images before and after fluid exchange show that CO_2 bubbles shrink upon exposure to air-equilibrated liquid but remain stable for hours. Also air bubbles in contact with CO_2-saturated water increase in size and Ostwald ripening occurs more rapidly due to the relatively high gas solubility of CO_2 in water.

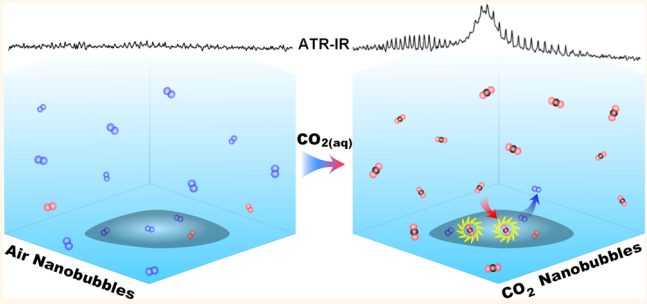

KEYWORDS: nanobubble stability · air/water interface · solvent exchange · Ostwald ripening · AFM · ATR-FTIR

The presence of nanobubbles was first proposed to explain long-range attractive interactions between two hydrophobic surfaces immersed in water.[1−3] This sparked debate for about a decade as to whether nanobubbles were stable enough to be observed.[1−5] Many measurements have shown that nanobubbles are indeed quite stable,[6−8] especially after procedures to induce gas supersaturation by solvent exchange,[7,9,10] electrochemical reactions,[11−13] or the plasmonic effect[14−16] are used to controllably produce them. As yet there is no widely accepted explanation for their stability. The theory of Epstein and Plesset, which is widely accepted to explain the growth and shrinkage of an isolated, stationary bubble in solution, predicts that nanobubbles should last less than a second.[17] This is in stark contrast to experimental observations that show they are stable for many minutes or up to several days.[18] Later Ljunggren and Eriksson using basically the same physical model but a different mathematical approach obtained the same result and pointed out that the predicted short lifetimes were incompatible with explanations for the hydrophobic interaction that were dependent upon the presence of surface nanobubbles.[19]

At least four different mechanisms have been proposed to explain the unexpectedly long lifetime of nanobubbles. It has been proposed that the gas/water interface of a nanobubble is shielded by a layer of impermeable contamination,[20] which leads to a drop in interfacial tension. The resulting near-zero Laplace pressure would be expected to eliminate the driving force for dissolution. This effect had previously been demonstrated by Berge *et al.* to stabilize micrometer-size bubbles in solutions of proteins.[21] However, it is clear that in the majority of nanobubble experiments such high levels of contamination are not present and are not responsible for nanobubble stability. Attempts to remove the putative impermeable skin by rinsing the system with surfactant solution have not led to nanobubble dissolution,[22] and the evidence

* Address correspondence to xuehuaz@unimelb.edu.au.

Received for review March 22, 2014 and accepted May 26, 2014.

Published online May 26, 2014
10.1021/nn5016049

is that the interfacial tension of a nanobubble in the absence of added surfactant is not low.[10] Lohse *et al.* proposed a dynamic equilibrium model in which the gas leaving the bubble is continuously replenished by the influx of gas.[23,24] This model predicts a liquid flow around the nanobubbles,[25] which though initially observed by lift mode AFM, was later determined by the authors to be due to incorrect measurements.[23] Furthermore, particle tracking measurements from this and other groups could not detect preferential flow around nanobubbles.[26,27] However, it is possible that the resolution of these measurements was insufficient to detect such preferential flow due to the relatively large size of the tracked particles (micrometers) compared to the nanobubbles. Recently it has been proposed that a thin layer of gas molecules on the surface may instead serve as a reservoir feeding gas to the nanobubbles.[28,29] This scenario contrasts with the mechanism by which nanobubbles are produced by the solvent exchange procedure, where the nanobubbles form from dissolved gas in the bulk liquid.[30] A third mechanism attributes nanobubble stability to the saturation of the dissolved gas and contact line pinning,[31−33] in which the height of bubbles changes while the lateral size remains constant. Calculations show that bubbles with a pinned three-phase boundary can survive much longer than free bubbles having the same volume. A supplementary mechanism, proposed by Weijs *et al.*, states that, in addition to pinning, a large number of nanobubbles on the surface locally increase the local gas supersaturation, such that the length scale over which molecules must diffuse is the size of the vessel and hence the lifetimes are extended.[32] Finally, two of us, in work that is yet to be published, propose an alternative theory for the rate of dissolution of a bubble that leads to lifetimes 3 orders of magnitude longer than the accepted theories.[17,19] Each of these explanations would result in a different rate of exchange of the gas between the bubble and the surrounding fluid, and therefore an experimental study of this exchange is warranted. Here we perform a set of experiments that attempt to determine if gas leaks from nanobubbles and the time scale over which leakage occurs.

To examine the leakage of nanobubbles, we employ attenuated total internal reflection Fourier transform infrared spectroscopy (ATR-FTIR) complemented by atomic force microscopy (AFM). Previously, Ducker and Zhang demonstrated that nanobubbles consisting of CO_2 can be detected in ATR-IR measurements.[18,34] This technique is able to distinguish between CO_2 molecules that are dissolved in liquid and those in the gaseous state. Spectra for CO_2 in the gaseous state exhibit rotational fine structure, which is absent when the gas is dissolved in a liquid due to the high rate of collisions. Conveniently, diatomic molecules such as N_2, O_2, and H_2 are not infrared active, so they do not appear in the ATR-IR spectra.

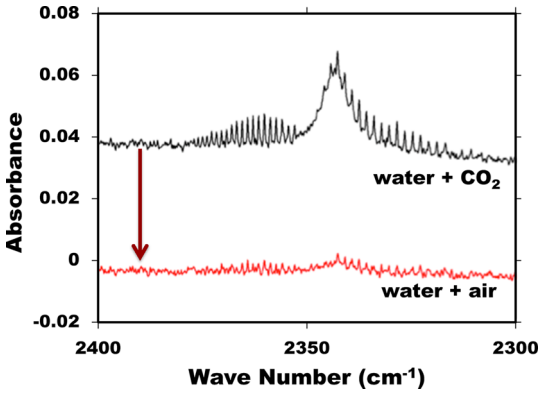

Figure 1. Infrared spectra of surface bubbles formed on OTS-Si in water+CO_2. Black: The spectrum after solvent exchange (the exchange of CO_2−ethanol by water+CO_2). Red: The spectrum after the water+CO_2 was replaced by the water+air after the formation of CO_2 bubbles. The background of each spectrum was collected in water+air. The gasous CO_2 absorption decreased signficantly after exposure to water+air, indicating the leakage of CO_2 gas molecules from the bubbles to water+air.

Our approach is twofold. First, we will expose surface nanobubbles containing diatomic (non-IR-active) gases to a solution containing dissolved CO_2 while capturing ATR-FTIR spectra in the 2500−2250 cm^{-1} range. If CO_2 enters the pre-existing nanobubbles, it will be revealed by the emergence of fine structure in the infrared spectra. Further, by studying the kinetics of the increase in the CO_2 signal we should be able to determine the exchange rate of aqueous CO_2 with the nanobubbles. If no CO_2 gas signal is seen, then we can conclude that surface nanobubbles are closed systems and gas exchange does not take place on the time scale of our experiments. Second, we will produce surface nanobubbles containing CO_2 gas, exchange the solvent until little CO_2 remains in solution, and then record ATR-FTIR spectra to follow any loss of CO_2 from the nanobubbles.

RESULTS

CO_2-Filled Nanobubbles. To assess the presence or absence of CO_2 in nanobubbles, difference IR spectra were obtained by subtracting spectra with added CO_2 from a background spectrum with air. For example, the fluid cell was filled with water+air and a background IR spectrum was obtained adjacent to the octamethyltrichlorosilane (OTS)-Si surface. An infrared spectrum was then obtained in CO_2-saturated water, and the background spectrum subtracted to give a difference spectrum. No gaseous CO_2 adsorption was observed. Then CO_2-filled nanobubbles were produced on the surface by solvent exchange using CO_2-saturated solvents. This time, absorption bands from gaseous CO_2 were observed in the difference spectrum (Figure 1, top), where the fine spectral lines are the signature of gaseous CO_2. Subsequently the water+CO_2 was gently replaced with water+air, and spectra were obtained as soon as possible afterward, which was some 3 min

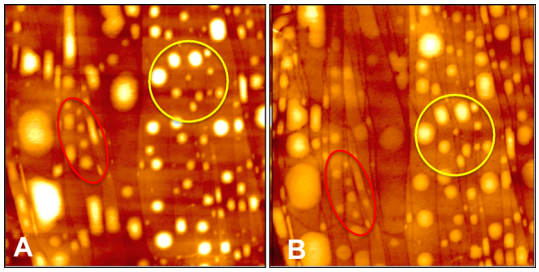

Figure 2. AFM height images of HOPG having a high surface coverage of bubbles in water+CO_2 and in water+air. (A) CO_2 bubbles that were produced and imaged in water+CO_2. (B) The same area as (A) ~20 min after water+CO_2 was replaced by the water+air. Scan size: 10 μm × 10 μm; height scale: 30 nm. The bubbles became flatter in water+air. Some bubbles are elongated, which is attributed to the pinning on the cleavage steps on the HOPG substrate. Two groups of the same nanobubbles are marked by yellow lines and by red lines in (A) and (B).

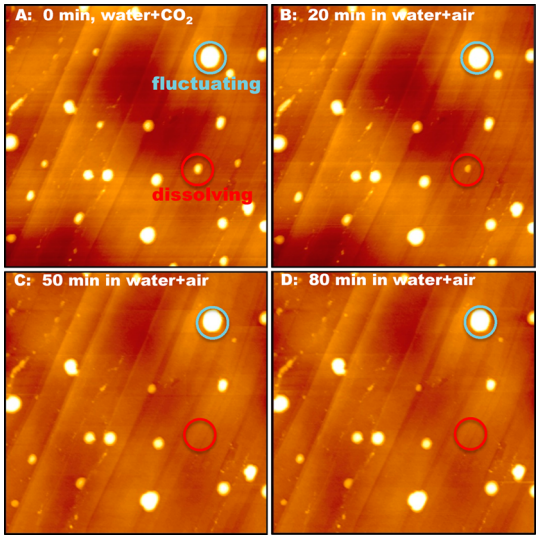

Figure 3. AFM images of HOPG having a low surface coverage of bubbles in water+CO_2 and in water+air. (A) Nanobubbles were produced in water+CO_2 by solvent exchange (the exchange of CO_2−ethanol by water+CO_2). Water+CO_2 was replaced by water+air, and then AFM images were acquired after 20 min (B), 50 min (C), and 80 min (D). Cyan and red circles are referenced in Figure 4. Scan size: 10 μm × 10 μm; height scale: 30 nm.

after exchange of solvents had commenced. Figure 1 (bottom) shows that already in the first spectrum after replacing the water+CO_2 the gaseous CO_2 peaks had nearly disappeared. This result is important, as it shows that the CO_2 gas molecules have diffused out of the interfacial nanobubbles upon exposure to water+air within 3 min. This observation contrasts sharply with what would be expected if an impermeable skin existed at the nanobubble surface to maintain nanobubble stability over multiple days. Instead, it shows that the nanobubble is an open system and that gas molecules rapidly transfer across the bubble's gas/liquid interface.

The complementary measurements by AFM were conducted after the exchange of ethanol+CO_2 by water+CO_2 was used to produce surface nanobubbles filled with CO_2. We selected two sets of AFM images on highly oriented pyrolytic graphite (HOPG) in Figures 2 and 3 that represent a high and a low initial surface coverage of nanobubbles in water+CO_2. When water+CO_2 was replaced gently with the water+air, the time between switching the liquid and the acquisition of the first AFM image was approximately 20 min. Both sets of AFM images show the same results: The majority of nanobubbles that formed in water+CO_2 remained on the surface after the replacement of water+CO_2 by water+air. This result indicates that in ATR-FTIR measurements the disappearance of gaseous CO_2 absorption bands after exposure of CO_2 bubbles to water+air was not due to the disappearance of nanobubbles, but due to the replacement of CO_2 inside the bubbles by non-IR-active gases in air, such as O_2 or N_2. The gaseous CO_2 molecules initially inside the bubbles had dissolved into the liquid phase. This is consistent with a two-way flow of gas molecules due to gradients in concentration. The CO_2 leaves the bubbles for the solution in which very little CO_2 is present, whereas the O_2 and N_2 gases leave the air-supersaturated solution by entering the nanobubble where initially there is no N_2 or O_2.

AFM images of nanobubbles on HOPG are shown in Figure 3. The initial bubbles are filled with CO_2. The solution is then changed to water+air, and images are obtained at the time intervals shown. The cross-sectional profiles of two representative bubbles indicated in Figure 3 are shown in Figure 4. The bubble in the red circle shrank in the first 20 min and completely dissolved before 50 min had elapsed, whereas the bubble in the cyan circle is relatively unchanged. It is notable that the contact line perimeter of the bubble in the red circle decreased with time, indicating that the bubble boundary had slipped as it dissolved in less than 50 min. Therefore, the strength of any pinning on the three-phase contact line was insufficient to keep the bubble boundary at its initial position up to the end of the bubble life.

Air-Filled Nanobubbles. We also conducted the alternative arrangement to the above experiments by examining air bubbles produced by the exchange of ethanol+air with water+air. Control experiments verified that bubbles were not formed when a dry substrate was immersed in water+air and that replacing water+air with water+CO_2 did not reveal spectral evidence of gaseous CO_2 when no nanobubbles were present. Although air bubbles formed by the exchange of ethanol+air by water+air could not be directly detected (because of the IR inactivity of the major atmospheric gases), the production of bubbles could be inferred by the negative peaks in the IR spectra corresponding to displacement of water by nanobubbles at the interface. As seen in Figure 5, replacing water+air with water+CO_2 led to the appearance of

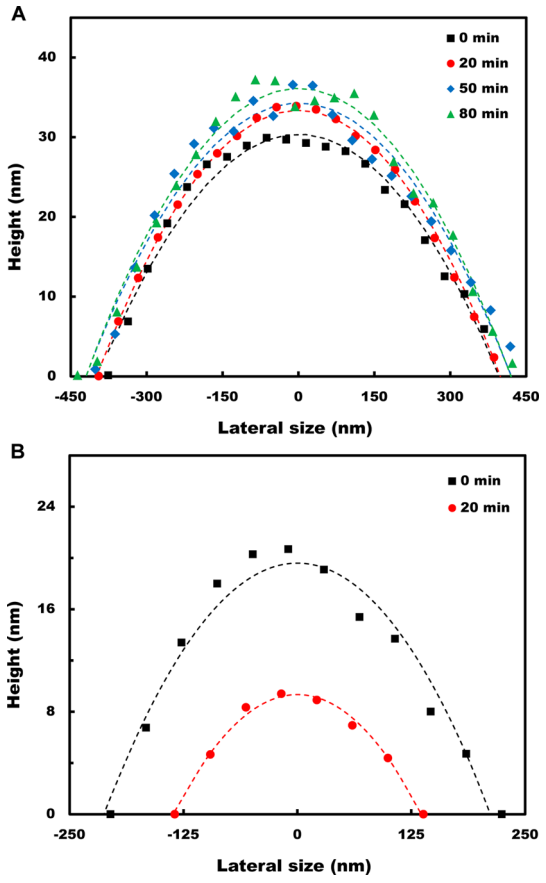

Figure 4. Cross-sectional profiles of bubbles circled in (A) cyan and (B) red in Figure 3. In water+air, the bubble circled in cyan stayed for over an hour, while the one circled in red disappeared within 50 min. The dashed lines are least-squares fits to spherical caps. The radii for each fit line was inserted into the Laplace equation to give the following pressures in atm: (A) 0 min, 1.55; 20 min, 1.59; 50 min, 1.55; 80 min, 1.58; (B) 0 min, 2.23; 20 min, 2.42.

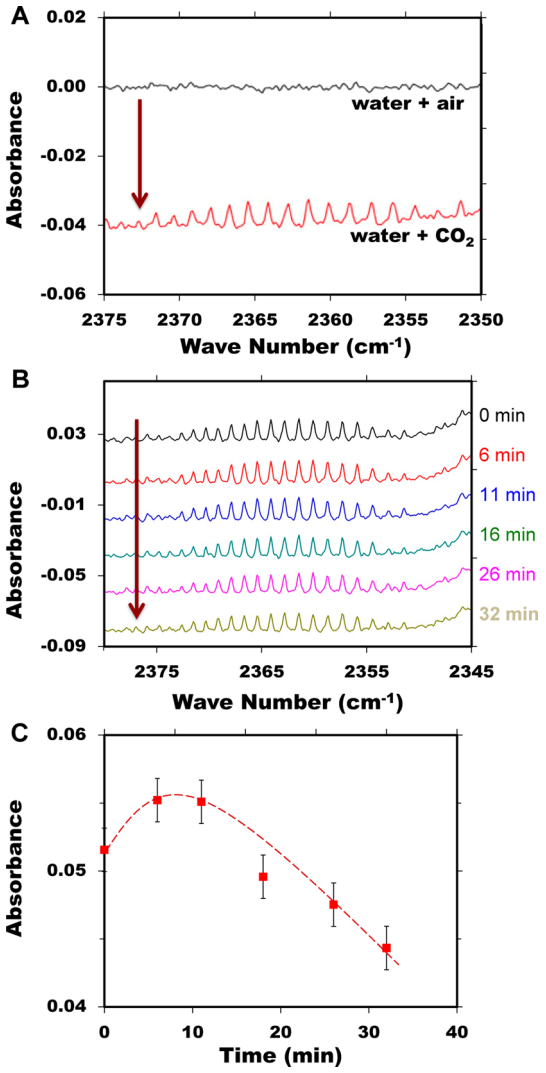

Figure 5. IR spectra of air bubbles exposed to water+CO_2. Air-containing nanobubbles were produced by the exchange of air−ethanol with water+air. (A) The spectrum (black) of air bubbles collected in water+air. No gaseous CO_2 spectra were observed. Then the water+air was replaced by water+CO_2, and gaseous CO_2 absorption bands were observed in the spectrum (red). (B) The spectrum in water+CO_2 shows that the gaseous CO_2 absorption bands decrease with time. (C) The sum of the height of the largest 10 peaks in the spectra obtained at different times. The dashed line emphasizes the initial increase and subsequent decrease in peak height with time. The error bars reflect uncertainty in the baseline and the height of the peaks.

CO_2 gaseous peaks in the first spectrum obtained. These results indicate that the presence of preformed nanobubbles by solvent exchange was essential for the detection of CO_2 gas molecules and that solvated CO_2 rapidly entered the preformed nanobubbles at the interface. These experiments support our earlier conclusions that the nanobubble interface is permeable to gas.

Figure 5C shows that the CO_2 gaseous peak intensities initially increased with time and then gradually decreased. This demonstrates that CO_2 gas molecules diffused both into and then out of the bubbles with time. This result is consistent with the previous observation that the intensity of the absorption due to gaseous CO_2 inside the nanobubbles decreases with time after their formation.[18]

To examine whether the amount of CO_2 entering the nanobubbles was related to the concentration of dissolved CO_2 in the liquid phase, water+CO_2 was diluted by different ratios of water+air before replacing the water+air. As seen in Figure 6, water+CO_2 diluted to 25% or 50% revealed no signs of gaseous CO_2 peaks, but some suggestion of gaseous CO_2 may be present for the *first* spectrum obtained at 75% dilution. These results show that the amount of CO_2 gas entering preformed air-filled nanobubbles is determined by the concentration of dissolved CO_2 in the liquid phase, which is consistent with diffusion of CO_2 from regions of high concentration to regions of low concentration.

Growth and shrinkage of air bubbles exposed to water+CO_2 is demonstrated by the AFM images shown in Figure 7. After water+CO_2 is added, the subsequent images reveal cases where nanobubbles shrink in size and dissolve (red circles) or fluctuate in size over time (cyan circles). These results indicate that

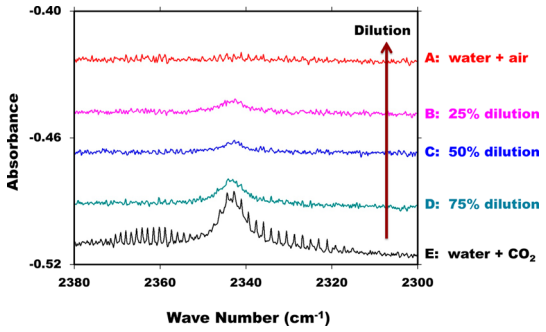

Figure 6. Diffusion of CO_2 from liquid phase to air nanobubbles. The infrared spectrum in water+air after the solvent exchange did not show gaseous CO_2 adsorbance (A). When the water+air was switched to water+CO_2, both gaseous CO_2 bands and aqueous CO_2 bands appeared in the spectrum (E). This demonstrates that the gaseous CO_2 diffused into the preformed air bubbles at the interface. If the water+CO_2 was diluted to 75% (D) before use, the bands from gaseous CO_2 were barely detectable after switching the liquid. The gaseous CO_2 bands were undetectable with the dilutions of 25% (B) or 50% (C).

CO_2 gas diffuses into the original air-filled nanobubbles. With time there was an overall reduction in the number density of nanobubbles. This contrasts with the long lifetime (several days) of nanobubbles in water+air reported in our earlier work[18] and demonstrates CO_2 nanobubbles are not as stable. This may be attributed to the solubility of CO_2 in water, which is much higher than other gases. We note that we did not control the level of supersaturation in these experiments, and it is possible that it is lower for CO_2.

Figure 8 shows the cross-sectional profiles of six representative bubbles labeled in Figure 7. All the bubbles initially grew in water+CO_2 (bubble 1−3 and a−c). Then after 20 more minutes, bubbles 1 and 3 dissolved entirely and bubble 2 shrank and then dissolved. The three bubbles labeled as a−c did not dissolve, but their heights fluctuated with time, perhaps due to variations in gas saturation levels resulting from temperature variations. The dashed lines were generated on the basis of least-squares fitting of the profile data to spherical caps. Assuming the Laplace equation applies,[35,36] we conclude the pressure differences associated with bubble curvature increase by as much as ~1 atm as the gas content of the fluids was exchanged.

We also examined the effects of salt on the permeability of the nanobubble interface. After producing air bubbles on the OTS-Si surface, the water+air solution was replaced with normal saline (NS, 0.9% NaCl solution). This solution was subsequently replaced with NS+CO_2, and ATR-FTIR spectra were obtained. The appearance of gaseous CO_2 signals shows that CO_2 had entered the nanobubbles from the NS+CO_2 solution (Figure 9).

DISCUSSION

Our measurements by ATR-FTIR and AFM show that CO_2-containing nanobubbles do not disappear upon exposure to water+air, but rather CO_2 gas molecules

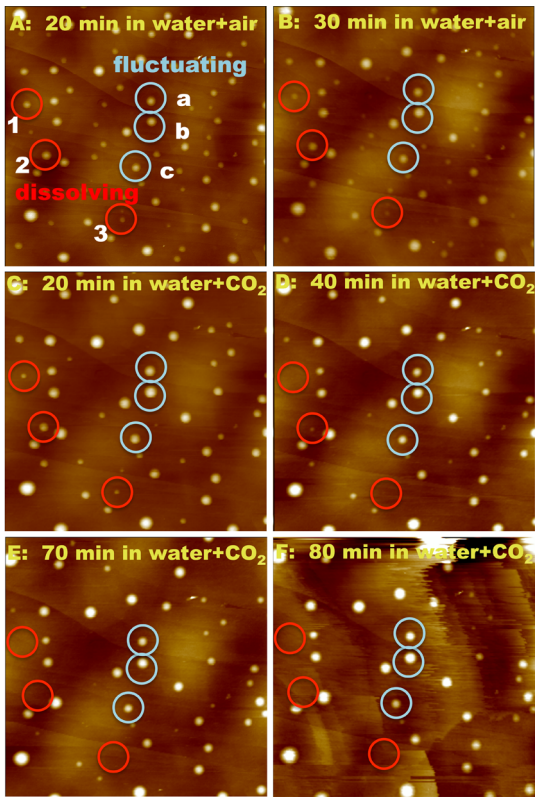

Figure 7. AFM images of air nanobubbles in water+CO_2. Air bubbles were produced by exchanging air−ethanol with water+air, and images obtained after 20 min (A) and 30 min (B). The water+air was then replaced with water+CO_2, and further images were obtained after 20 min (C), 40 min (D), 70 min (E), and 80 min (F). Red circles indicate dissolving bubbles, and cyan circles indicate bubbles that remain stable but fluctuate in size over time. For all images, scan size: 10 μm × 10 μm; height scale: 30 nm.

inside the nanobubbles leak out into the water. Similarly, air bubbles at the interface also take in CO_2 molecules from the liquid phase. Clearly the gas/water interface of nanobubbles is permeable; that is, gas molecules inside the bubbles are exchanging with the dissolved gas in the liquid. The permeability of the interface to gas is also maintained in the presence of salt. The exchange rates observed in this study ($t_{1/2}$ < 1 min) cannot be accurately determined because gases have almost completely exchanged prior to the first measurement. Further support for the permeability of nanobubbles is seen in the pronounced Ostwald ripening that takes place in CO_2-saturated water, as well as the growth and shrinkage of nanobubbles under external fields.[18,33,37] Therefore, an impermeable skin at the nanobubble surface can be ruled out as a general mechanism for nanobubble stability.

We note here that the gradient in CO_2 concentration is high, as it is initially present in significant quantities in one of the phases. The large gradient will lead to faster diffusion, and therefore the kinetics of CO_2 exchange in the Ostwald ripening is expected to be much higher than for air nanobubbles of different sizes in water+air solutions.

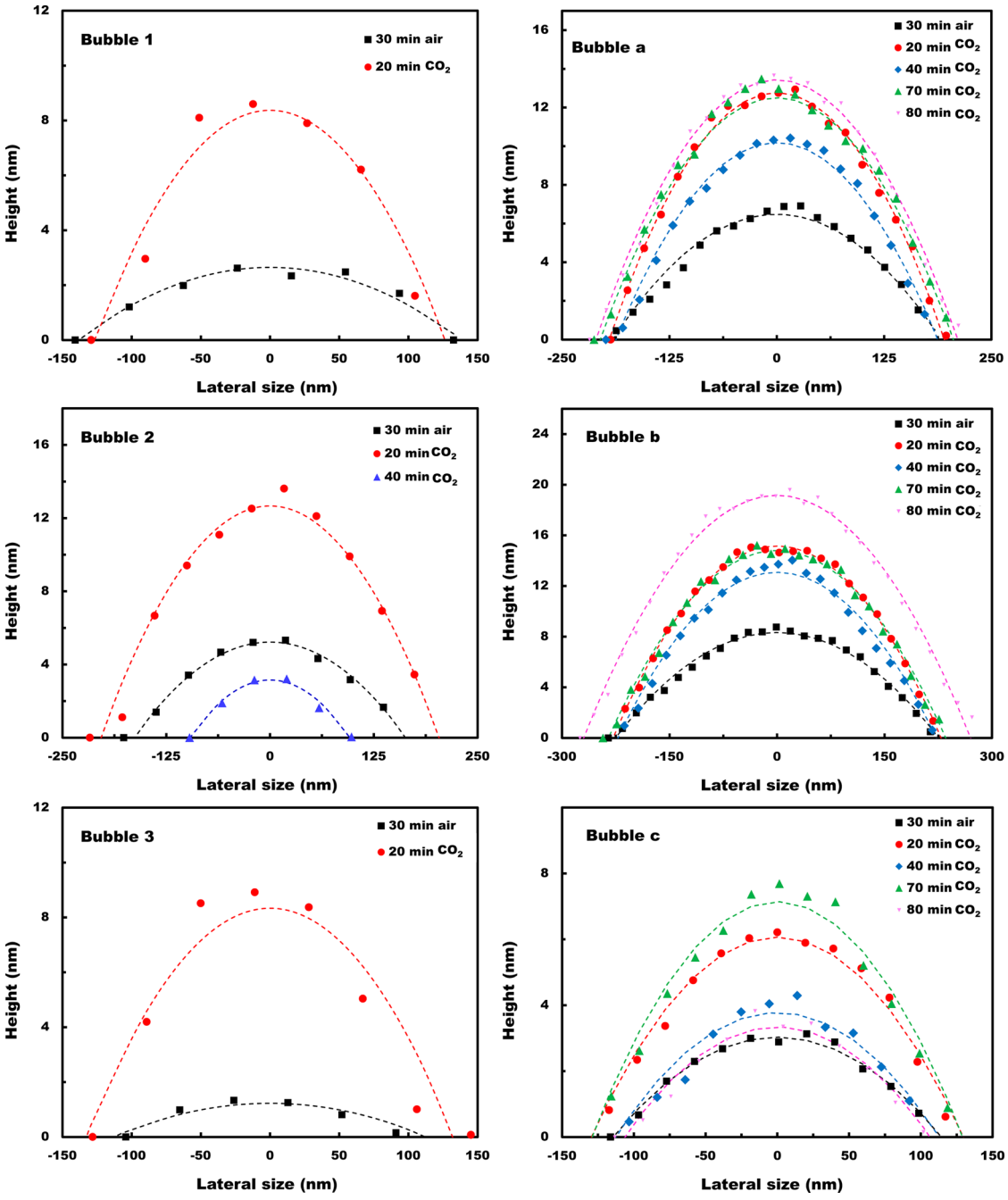

Figure 8. Cross-sectional profiles of the bubbles labeled in Figure 7. In water+CO_2, bubbles 1−3 disappeared with time, bubbles a−c still remained, but their heights were fluctuating. The dashed lines are least-squares fits to spherical caps. The radius for each fit line was inserted into the Laplace equation to give the following pressures in atm: (1) 30 min, 1.39; 20 min, 2.46; (2) 30 min, 1.55; 20 min, 1.86; 40 min, 1.96; (3) 30 min, 1.27; 20 min, 2.34; (a) 30 min, 1.50; 20 min, 1.95; 40 min, 1.82; 70 min, 1.84; 80 min, 1.86; (b) 30 min, 1.46; 20 min, 1.82; 40 min, 1.75; 70 min, 1.76; 80 min, 1.74; (c) 30 min, 1.66; 20 min, 2.02; 40 min, 1.84; 70 min, 2.21; 80 min, 1.84.

The stability of CO_2 nanobubbles has shown individuality: some dissolve, others do not, and the dissolution rate is different for different bubbles. Diversity of nanobubble evolution has been observed in several other circumstances. For example, some nanobubbles grow and other nanobubbles remain unchanged after depressurization.[38] Under perturbation by the tip of an AFM cantilever some nanobubbles disappeared, while others moved along the surface.[38] So far, no theory has been proposed to explain why individual nanobubbles behave differently.

Pinning effects together with gas supersaturation in the liquid are the main elements in the mechanisms recently proposed for nanobubble stability.[31−33] The theory of Epstein and Plesset[17] predict that for an isolated, stationary, single spherical bubble with a radius of 2.6 μm, it takes only 1 s for the bubble to deflate under a gas saturation level of 0.99. In recent

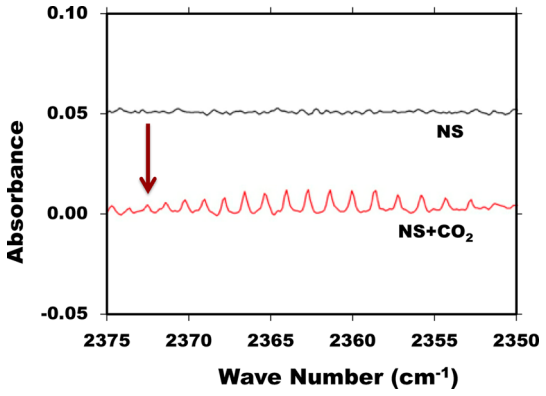

Figure 9. Diffusion of CO_2 from salt solutions into air bubbles. After forming bubbles though solvent exchange, the air-equilibrated water was replaced by NS to obtain the black spectrum. The bubbles were then exposed to NS+CO_2, and the red spectrum was collected. The gaseous CO_2 signals indicate that CO_2 diffused from NS+CO_2 into preformed bubbles.

work, the Epstein and Plesset model has been applied to surface nanobubbles by Zhang *et al.*[33] and by Weijs and Lohse.[32] The pool depth is a key parameter in the model by Weijs and Lohse[32] and is unknown in our experiments. Therefore, we apply the model by Zhang *et al.*[33] to estimate the lifetime of surface nanobubbles. Under the same saturation level of 0.99, this modified Epstein and Plesset model predicts lifetimes as long as 200 s for nanobubbles 20 nm in height. The modified Epstein and Plesset model assumes that gas pressures remain constant due to the relatively flat shape of the nanobubbles. But, the difficulty for this modified Epstein and Plesset model is that nanobubble lifetimes are predicted to be extremely sensitive to gas supersaturation levels as they approach 1, which has not been observed experimentally. The lifetimes of the nanobubbles we observe are much longer than these theories predict. Similarly, the rates of CO_2 exchange we observe are much slower than what would be expected from the dynamic equilibrium model.[24,25]

In these experiments we observe long-lived nanobubbles in which the three-phase line does not move and others in which the three-phase line retreats as the bubble dissolves. With regard to pinning this can be interpreted in two ways. One could conclude that pinning is an important factor in reducing the rate of dissolution of nanobubbles. When the bubbles are shrinking in a way that the three-phase line is moving over time, this explanation requires a consideration of the time fraction for which the three-phase contact line is in a pinned or unpinned state. According to accepted theory,[17,19] if the bubble is unpinned for a fraction of a second, the bubble will dissolve. A scenario could be proposed that as the three-phase line moves, it is doing so in a series of short steps separated by longer pinned stages, with the result that it is pinned close to 100% of the time. Alternatively, one could conclude that for the bubbles in which the three-phase line is moving their stability is not related to pinning.

Our results show that the presence of salt in the solution did not prevent gas exchange between bubbles and the dissolved gases in the liquid phase even though several papers have proposed that the stability of bulk nanobubbles is due to the ionic shells provided by salts in the solution.[33,39−44] As the gas−water interface of a surface nanobubble is expected to be the same as for a nanobubble in the bulk, the inference is that nanobubbles in bulk also have permeable interfaces. Therefore, we conclude that for bulk nanobubbles that are of comparable size (there are many reports of ~100 nm size bulk nanobubbles) it is likely that salt does not stabilize them.

CONCLUSIONS

In summary, a combination of ATR-FTIR and AFM measurements has shown that gas can readily pass through the liquid−gas interface of a nanobubble. Such gas exchange is revealed by following gaseous CO_2 spectra in different liquid media. Dissolved CO_2 in the liquid readily enters into preformed air-filled surface nanobubbles. Likewise, CO_2 gas molecules inside nanobubbles readily dissolve into air-equilibrated water. AFM images show that CO_2 bubbles remain on the surface upon exposure to air-equilibrated liquid. Air bubbles in contact with CO_2-saturated water first grow then shrink, and some eventually dissolve with time in CO_2-saturated water possibly assisted by the high gas solubility of CO_2 in water. The presence of salt in the solution does not prevent gas leakage from nanobubbles.

This work clearly addresses the models proposed to explain nanobubble stability. The results presented here suggest a free exchange of gases with the bulk solution and are therefore inconsistent with models that preclude gas exchange. The results also provide some evidence that gas saturation levels are important to nanobubble stability. We conclude that an impermeable skin cannot be a general mechanism for nanobubble stability. Furthermore, important elements of other published mechanisms proposed as general descriptors for nanobubble stability are not supported by our results.

METHODS

Chemicals and Materials. All water used was purified using a Milli-Q unit and was stored at 4 °C overnight before being warmed to 37 °C immediately before use. This will lead to supersaturation of air in the water. All ethanol used was distilled. Normal saline was purchased from Hospira (0.9% NaCl for irrigation, USP pH 5.6). CO_2-saturated NS was produced by 20 min or more of bubbling of gaseous CO_2 supplied from a high-purity gas cylinder, further purified through a water bath. Teflon tubes and glass syringes were used in handling the liquids.

Silicon wafers, silanized with octamethyltrichlorosilane to render them hydrophobic, were prepared by following the protocol in the literature.[10,45,46] The OTS-Si substrates produced had an advancing contact angle of 110° for water and a receding contact angle of 95−100°.

A purpose-built ATR cell was used with the hydrophobized silicon wafer as the light-guiding prism. In our ATR configuration, the penetration depth in water is about 250 nm at 2500 cm^{-1}. The substrate was cleaned in toluene, acetone, ethanol, and water subsequently by ultrasound for 15 min before it was mounted into the ATR fluid cell in a laminar cabinet. The fluid cell was sealed except for an inlet and outlet connected to Teflon tubes. In the standard solvent exchange procedure, ethanol was injected into the fluid cell and then gently replaced by water. The measurements were conducted at room temperature, and the ethanol and water were heated to 37 °C prior to solvent exchange. The liquid was injected to the fluid cell from a 2.5 mL glass syringe by hand as slowly as possible. When connecting the syringe to the inlet tube, air bubbles were avoided completely.

Atomic force microscopy measurements were conducted using a Multimode Nanoscope IIIa (Bruker, MA, USA) within a closed glass fluid cell. A silicone O-ring was used to seal the fluid cell. The procedure for solvent exchange was the same as in the ATR-FTIR experiments and also as in our previous work.[10,19,34,39] The flow rate was also kept as slow as possible during the injection by hand. Silicon nitride cantilevers (OMCL-TR, Olympus) with a typical spring constant of 0.08 N/m and resonance of 34 kHz were used for imaging. The cantilever and the fluid cell were cleaned by oxygen plasma before use. Images were collected in tapping mode on HOPG surfaces because a high number density of nanobubbles makes it easier to find nanobubbles in probed areas. Nanobubbles were observed on both OTS-Si and HOPG surfaces, but higher quality images were obtained using HOPG. CO_2-filled bubbles were formed by the exchange of CO_2-supersaturated ethanol by CO_2-supersaturated water (subsequently called water+CO_2). The CO_2-supersaturated solutions were prepared by bubbling CO_2 through the solvent for 20 min. The air-containing nanobubbles were produced by solvent exchange of air-supersaturated ethanol by air-supersaturated water (subsequently called water+air).

Conflict of Interest: The authors declare the following competing financial interest(s): Sean German and Tony Mega are employees of Revalesio Corporation.

Acknowledgment. This work is part of the program "Are Nanobubbles Leaky?" funded by Revalesio Corporation. X.H.Z. gratefully acknowledges the support from ARC Future Fellowship Scheme (FFT120100473).

REFERENCES AND NOTES

1. Parker, J. L.; Claesson, P. M.; Attard, P. Bubbles, Cavities, and the Long-Ranged Attraction Between Hydrophobic Surfaces. *J. Phys. Chem.* **1994**, *98*, 8468–8480.
2. Poynor, A.; Hong, L.; Robinson, I.; Granick, S.; Zhang, Z.; Fenter, P. How Water Meets a Hydrophobic Surface. *Phys. Rev. Lett.* **2006**, *97*, 266101.
3. Carambassis, A.; Jonker, L.; Attard, P.; Rutland, M. Forces Measured between Hydrophobic Surfaces Due to a Submicroscopic Bridging Bubble. *Phys. Rev. Lett.* **1998**, *80*, 5357–5360.
4. Doshi, D. A.; Watkins, E. B.; Israelachvili, J. N.; Majewski, J. Reduced Water Density at Hydrophobic Surfaces: Effect of Dissolved Gases. *Proc. Natl. Acad. Sci. U.S.A.* **2005**, *102*, 9458–9462.
5. Meyer, E. E.; Rosenberg, K. J.; Israelachvili, J. Recent Progress in Understanding Hydrophobic Interactions. *Proc. Natl. Acad. Sci. U.S.A.* **2006**, *103*, 15739–15746.
6. Ishida, N.; Inoue, T.; Miyahara, M.; Higashitani, K. Nano Bubbles on a Hydrophobic Surface in Water Observed by Tapping-Mode Atomic Force Microscopy. *Langmuir* **2000**, *16*, 6377–6380.
7. Lou, S.-T.; Ouyang, Z.-Q.; Zhang, Y.; Li, X.-J.; Hu, J.; Li, M.-Q.; Yang, F.-J. Nanobubbles on Solid Surface Imaged by Atomic Force Microscopy. *J. Vac. Sci. Technol. B* **2000**, *18*, 2573–2575.
8. Tyrrell, J. W.; Attard, P. Images of Nanobubbles on Hydrophobic Surfaces and Their Interactions. *Phys. Rev. Lett.* **2001**, *87*, 176104.
9. Yang, J.; Duan, J.; Fornasiero, D.; Ralston, J. Very Small Bubble Formation at the Solid-Water Interface. *J. Phys. Chem. B* **2003**, *107*, 6139–6147.
10. Zhang, X. H.; Maeda, N.; Craig, V. S. J. Physical Properties of Nanobubbles on Hydrophobic Surfaces in Water and Aqueous Solutions. *Langmuir* **2006**, *22*, 5025–5035.
11. Liu, G.; Wu, Z.; Craig, V. S. Cleaning of Protein-Coated Surfaces Using Nanobubbles: An Investigation Using a Quartz Crystal Microbalance. *J. Phys. Chem. C* **2008**, *112*, 16748–16753.
12. Wu, Z.; Chen, H.; Dong, Y.; Mao, H.; Sun, J.; Chen, S.; Craig, V. S. J.; Hu, J. Cleaning Using Nanobubbles: Defouling by Electrochemical Generation of Bubbles. *J. Colloid Interface Sci.* **2008**, *328*, 10–14.
13. Zhang, L.; Zhang, Y.; Zhang, X.; Li, Z.; Shen, G.; Ye, M.; Fan, C.; Fang, H.; Hu, J. Electrochemically Controlled Formation and Growth of Hydrogen Nanobubbles. *Langmuir* **2006**, *22*, 8109–8113.
14. Polman, A. Solar Steam Nanobubbles. *ACS Nano* **2013**, *7*, 15–18.
15. Neumann, O.; Feronti, C.; Neumann, A. D.; Dong, A.; Schell, K.; Lue, B.; Kim, E.; Quinn, M.; Thompson, S.; Grady, N.; *et al.* Compact Solar Autoclave Based on Steam Generation Using Broadband Light-Harvesting Nanoparticles. *Proc. Natl. Acad. Sci. U.S.A.* **2013**, *110*, 11677–11681.
16. Neumann, O.; Urban, A. S.; Day, J.; Lal, S.; Nordlander, P.; Halas, N. J. Solar Vapor Generation Enabled by Nanoparticles. *ACS Nano* **2013**, *7*, 42–49.
17. Epstein, P. S.; Plesset, M. S. On the Stability of Gas Bubbles in Liquid-Gas Solutions. *J. Chem. Phys.* **1950**, *18*, 1505–1509.
18. Zhang, X. H.; Quinn, A.; Ducker, W. A. Nanobubbles at the Interface between Water and a Hydrophobic Solid. *Langmuir* **2008**, *24*, 4756–4764.
19. Ljunggren, S.; Eriksson, J. C. The Lifetime of a Colloid-Sized Gas Bubble in Water and the Cause of the Hydrophobic Attraction. *Colloid Surf. A* **1997**, *129−130*, 151–155.
20. Ducker, W. Contact Angle and Stability of Interfacial Nanobubbles. *Langmuir* **2009**, *25*, 8907.
21. Berge, L. I. Dissolution of Air Bubbles by the Resistive Pulse and the Pressure Reversal Technique. *J. Colloid Interface Sci.* **1990**, *134*, 548–562.
22. Zhang, X.; Uddin, M. H.; Yang, H.; Toikka, G.; Ducker, W.; Maeda, N. Effects of Surfactants on the Formation and the Stability of Interfacial Nanobubbles. *Langmuir* **2012**, *28*, 10471–10477.
23. Seddon, J. R. T.; Lohse, D. Nanobubbles and Micropancakes: Gaseous Domains on Immersed Substrates. *J. Phys: Condens. Matter* **2011**, *23*, 133001.
24. Brenner, M.; Lohse, D. Dynamic Equilibrium Mechanism for Surface Nanobubble Stabilization. *Phys. Rev. Lett.* **2008**, *101*, 214505.
25. Seddon, J. R. T.; Zandvliet, H. J. W.; Lohse, D. Knudsen Gas Provides Nanobubble Stability. *Phys. Rev. Lett.* **2011**, *107*, 116101.
26. Chan, C. U.; Ohl, C.-D. Total-Internal-Reflection-Fluorescence Microscopy for the Study of Nanobubble Dynamics. *Phys. Rev. Lett.* **2012**, *109*, 174501.
27. Dietrich, E.; Zandvliet, H. J. W.; Lohse, D.; Seddon, J. R. T. Particle Tracking around Surface Nanobubbles. *J. Phys: Condens. Matter* **2013**, *25*, 184009.
28. Peng, H.; Hampton, M. A.; Nguyen, A. V. Nanobubbles Do Not Sit Alone at the Solid−Liquid Interface. *Langmuir* **2013**, *29*, 6123–6130.
29. Lu, Y.-H.; Yang, C.-W.; Hwang, I.-S. Molecular Layer of Gaslike Domains at a Hydrophobic-Water Interface Observed by Frequency-Modulation Atomic Force Microscopy. *Langmuir* **2012**, *28*, 12691–12695.
30. Lhuissier, H.; Lohse, D.; Zhang, X. Spatial Organization of Surface Nanobubbles and Its Implications in Their Formation Process. *Soft Matter* **2014**, *10*, 942.

31. Liu, Y.; Zhang, X. Nanobubble Stability Induced by Contact Line Pinning. *J. Chem. Phys.* **2013**, *138*, 014706.
32. Weijs, J. H.; Lohse, D. Why Surface Nanobubbles Live for Hours. *Phys. Rev. Lett.* **2013**, *110*, 054501.
33. Zhang, X.; Chan, D. Y. C.; Wang, D.; Maeda, N. Stability of Interfacial Nanobubbles. *Langmuir* **2013**, *29*, 1017–1023.
34. Zhang, X.; Khan, A.; Ducker, W. A Nanoscale Gas State. *Phys. Rev. Lett.* **2007**, *98*, 136101.
35. Attard, P. Nanobubbles and the Hydrophobic Attraction. *Adv. Colloid Interface Sci.* **2003**, *104*, 75–91.
36. Nagayama, G.; Tsuruta, T.; Cheng, P. Molecular Dynamics Simulation on Bubble Formation in a Nanochannel. *Int. J. Heat Mass Transfer* **2006**, *49*, 4437–4443.
37. Brotchie, A.; Zhang, X. H. Response of Interfacial Nanobubbles to Ultrasound Irradiation. *Soft Matter* **2011**, *7*, 265.
38. Zhang, X. H.; Li, G.; Maeda, N.; Hu, J. Removal of Induced Nanobubbles from Water/Graphite Interfaces by Partial Degassing. *Langmuir* **2006**, *22*, 9238–9243.
39. Jin, F.; Li, J.; Ye, X.; Wu, C. Effects of pH and Ionic Strength on the Stability of Nanobubbles in Aqueous Solutions of A-Cyclodextrin. *J. Phys. Chem. B* **2007**, *111*, 11745–11749.
40. Jin, F.; Gong, X.; Ye, J.; Ngai, T. Direct Measurement of the Nanobubble-Induced Weak Depletion Attraction between a Spherical Particle and a Flat Surface in an Aqueous Solution. *Soft Matter* **2008**, *4*, 968–971.
41. Ohgaki, K.; Khanh, N.; Joden, Y.; Tsuji, A. Physicochemical Approach to Nanobubble Solutions. *Chem. Eng. Sci.* **2010**, *65*, 1296–1300.
42. Oeffinger, B. E.; Wheatley, M. A. Development and Characterization of a Nano-Scale Contrast Agent. *Ultrasonics* **2004**, *42*, 343–347.
43. Kozempel, S.; Tauer, K.; Rother, G. Aqueous Heterophase Polymerization of Styrene—a Study by Means of Multi-Angle Laser Light Scattering. *Polymer* **2005**, *46*, 1169–1179.
44. Dube, N. K.; Oeffinger, B. E. Development and Characterization of a Nano-Sized Surfactant Stabilized Contrast Agent for Diagnostic Ultrasound. *Proc. IEEE 29th Ann. Northeast Bioeng. Conf.* **2003**, 102–103.
45. Wang, M.; Liechti, K. M.; Wang, Q.; White, J. M. Self-Assembled Silane Monolayers: Fabrication with Nanoscale Uniformity. *Langmuir* **2005**, *21*, 1848–1857.
46. Wang, Y.; Lieberman, M. Growth of Ultrasmooth Octadecyltrichlorosilane Self-Assembled Monolayers on SiO_2. *Langmuir* **2003**, *19*, 1159–1167.